

## SCREW SWIRLING EFFECTS ON FIBER ORIENTATION DISTRIBUTION IN LARGE-SCALE POLYMER COMPOSITE ADDITIVE MANUFACTURING

Zhaogui Wang\*, Douglas E. Smith\*

\*Department of Mechanical Engineering, Baylor University, Waco, TX 76798

### Abstract

Large-Scale Additive Manufacturing (LSAM) polymer deposition employs a single screw extruder to melt and deliver the pelletized feedstock resulting in significantly higher flow rates as compared to conventional filament-extrusion AM processes. Single screw swirling motion in the melt flow during processing generates a unique pattern of flow-induced fiber alignment when fiber-filled polymer feedstock is processed. This paper investigates the effect of the single screw swirling motion on the fiber orientation and predicted elastic properties of a printed extrudate. A finite element extruder nozzle flow is created, where the extruder screw tip, the extrusion nozzle, and a short section of free extrudate compose the melt flow domain. The IRD-RSC fiber orientation diffusion model is applied to capture the slow orientation kinetics of short fibers in the concentrated fiber suspension. The results indicate that the swirling motion of the flow has a direct effect on predicted fiber orientation distribution and the associated averaged elastic properties in the extruded composite bead.

### Introduction

Polymer deposition Additive Manufacturing (AM) (otherwise known as fused filament fabrication or fused deposition modeling) has been extended from moderate-size rapid prototyping to the manufacture of large-scale end use parts and tooling. Unlike conventional polymer extrusion additive processes where wire-shape filament feedstock is typically used, LSAM polymer composite deposition processes utilizes a single screw extruder to melt and extrude pelletized feedstock which results in a significant increase in the flow rate and enables the fabrication of larger structures.

Prior studies show the rotating screw has a direct effect on the material behaviors of a fiber-polymer suspension in polymer processing applications. Zhou, et al. [1] investigated the variation of polymer viscosity during processed by a single screw extruder using finite element suite ANSYS Polyflow. It was found that the viscosity dropped initially and then tended to a stable value as processing continued. This trend happened periodically and was related to the geometry of the screw. Michelangelli, et al. [2] studied the process of single screw melting pelletized feedstock using the Discrete Element Method (DEM) and their numerical results achieved a good agreement with published data. Canevarolo, et al. [3] studied the effects of screw element type on degrading Polypropylene (PP). Five different screw designs were considered and it was found that increasing the screw number as well as the screw profile aggressiveness yielded a noticeable reduction in the average molecular weight of PP. Kelly, et al. [4] measured the melt temperature profiles in single screw extrusion flow using different screw geometries and found that a barrier lighted screw provided preferable melting conditions, especially at higher processing speeds.

Ramani, et al. [5] investigated the fiber length degradation in a twin screw extruder and found that the injection molding process did not benefit from the wet-out and dispersion of fiber reinforcements. Covas, et al. [6] investigated the rheology properties of the fiber-polymer mixed compounds with three different screw geometry designs. They found that the screw geometry design had slight effect on the probability of fiber breakage. More recently, Duty, et al. [7] measured the elastic stiffness of fiber filled polymers printed through a LSAM system. The stiffness of the extruded material showed a high degree of anisotropy, where the material modulus along the printing direction is much higher than that transverse to the axis of the bead. Duty, et al [7] also showed that different designs of the screw (see Figure 1) affects the resulting elastic properties of the printed materials significantly, as appearing in Table 1, where the modulus of the printed polymer composite bead along the bead direction decreased significantly when the process was switched to retrofit screw from original screw.

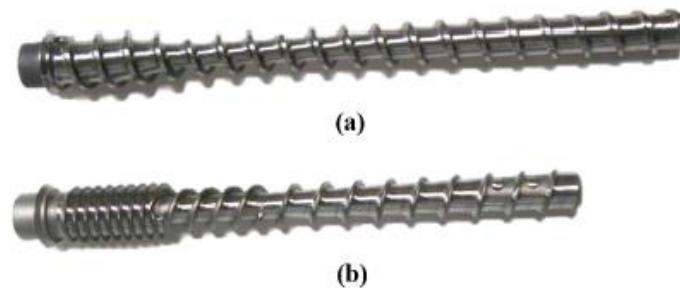


Figure 1. Different designs of the single screw used for a LSAM system: (a) custom-designed retrofit screw; (b) original Dohle extrusion screw [7].

Table 1. Stiffness of composite materials processed by different screws [7].

Material	Screw design	Modulus at printing direction (GPa)	Modulus at transverse direction (GPa)
20% Glass fiber-filled ABS	Original	5.67	2.45
20% Glass fiber-filled ABS	Retrofit	3.33	1.71
20% Carbon fiber-filled ABS	Original	11.94	2.13
20% Carbon fiber-filled ABS	Retrofit	6.33	2.04

A few factors are considered to have attributed the results shown in Table 1. Firstly, the flow-induced fiber orientation, which has been universally acknowledged as the main contributing factor for defining mechanical properties of a short fiber polymer composite material processed through certain polymer processing method [8], is considered to experience some variation when different screws are applied. Besides, it is also believed that some degree of fiber breakage occurs during the screw extrusion process, which contributes to the changing of the material properties [5].

The primary objective of this paper is to characterize the effects of the screw swirling motion on the predicted fiber orientation in an extruded short fiber polymer composite produced through LSAM extrusion. To address this issue, we consider a polymer melt flow model using the well-established finite element suite ANSYS Polyflow (ANSYS, Inc., Canonsburg, PA, USA).

The flow model includes a short section of the extruder that connects the nozzle die, the nozzle portion, and a short strand of a vertical extrudate. To investigate if the rotating screw plays a critical role in the fiber orientation prediction, two types of flow models are created: 1) a swirling flow model and 2) a straight flow model, as appearing in Figure 2, (c) and (d), respectively. A weakly coupled one-way analysis is then performed to compute the fiber orientation based on the velocity gradients computed in the melt flow simulation. We employ the Isotropic Rotary Diffusion Reduced Strain Closure (IRD-RSC) model [9] to capture the slow orientation kinetics of the reinforced short fibers in the polymer melt. Effective elastic constants of a printed composite extrudate bead is also evaluated using the orientation homogenization method [10-12] for the computed steady-state orientation state.

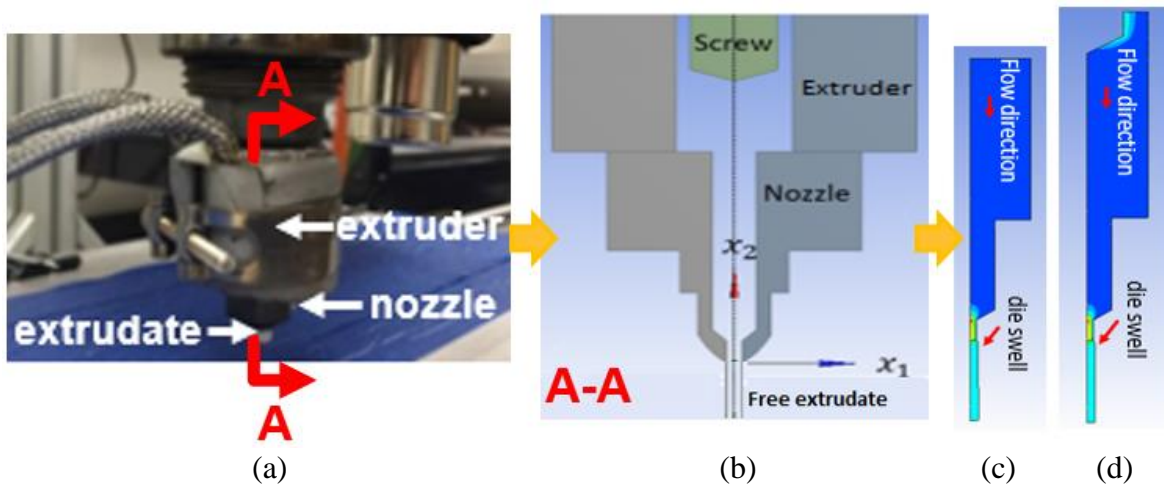


Figure 2. (a) LSAM polymer deposition process; (b) the melt flow domain of interest; (c) straight flow model; (d) swirling flow model.

## Methodology

The simulations presented below will consider a 13% Carbon Fiber filled Acrylonitrile Butadiene Styrene (CF-ABS) which is a material that is typically used in LSAM applications. The fluid rheology properties of the molten feedstock is measured by a frequency sweep using a HAAKE MARS 40 rheometer. We consider the Phan-Thien-Tanner model (PTT) [13] viscoelastic fluid model where material constants are computed from the experimental data. These rheology properties serve as input to our ANSYS Polyflow extrusion model where fiber orientation is computed once the flow kinematics are obtained. Finally, the effective stiffness of an extruded bead of polymer composite is computed by an orientation homogenization method.

### Material Rheology Model

In this paper, 13% CF-ABS is selected since it is commonly used in LSAM polymer deposition systems. The Phan-Thien-Tanner (PTT) model [14] is regarded as one of the most realistic rheology models for polymer melt flow computation, and thus is selected for our LSAM polymer extrusion study. We obtain the oscillation fluid properties of the 13% CF-ABS through a frequency sweep test (0.01 Hz – 100 Hz) in a rotational rheometer MARS 40. A parameter fitting procedure is performed in ANSYS Polymath where the results are given in Figure 3. Results

obtained through the MARS 40 oscillatory rheometer frequency sweep test are converted to a function of shear rate by applying the Cox-Merz rule [15] where data is obtained over a shear rate ranged of  $0.0628 \text{ s}^{-1}$  to  $628 \text{ s}^{-1}$ . A five-mode PTT model is considered where we assign the relaxation time as  $10^{-3} \text{ s}$  to  $10^1 \text{ s}$ , increasing one order of magnitude for each mode. The other parameters associated with the rheology model remain the default setting. Finally, an automate fitting procedure is performed where the fitted results of the PTT model appear in Table 2. Also,  $1/9$  of the viscosity constant in the first mode of the fitted PTT model is assigned as a Newtonian component to improve numerical stability as suggested by ANSYS Polyflow [14]. In addition, PTT model uses two constant parameters  $\xi$  and  $\varepsilon$  to control the shear thinning viscosity and extensional viscosity behaviors [14]. The fitted results shown in Figure 3 are obtain with  $\xi=0.15$  and  $\varepsilon=0.5$  through the data fitting procedure.

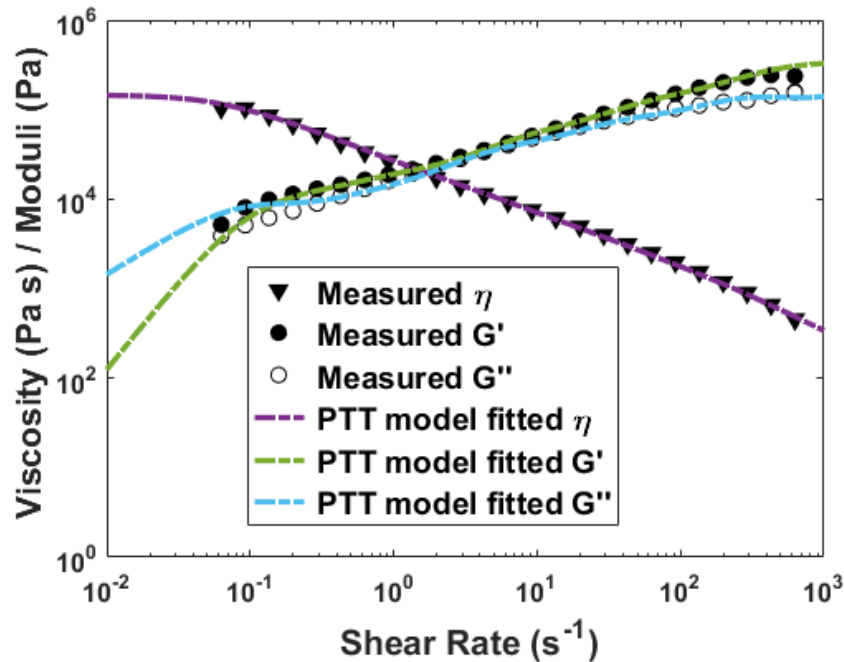


Figure 3. Rheology properties from fitted fluid models and experimental measurement.

Table 2. Fitted parameters for the five-mode PTT model.

$i$	$\lambda_i(\text{s})$	$\eta_i(\text{Pa} \cdot \text{s})$
1	0.0032	719.238
2	0.024	2009.14
3	0.17	6812.35
4	1.37	11716.6
5	10.00	124392

### Melt Flow Simulation

Polymer melt flow models are created based on the geometrical design of a LSAM Strangpresse Model-19 extruder. The straight flow and the swirling flow share the same dimensions, except that the straight flow starts from the tip of the screw edge without consideration of the rotating motion. The swirling flow model includes the ending section of the extruder, where

the flow near the edge of the rotating screw tip is included in the simulation. the flow domain also includes the nozzle flow and a short section of free extrudate outside the nozzle exit. The dimensional detail of the flow model is given in Figure 4. Note, due to the axisymmetry feature, we consider only half of the flow domain using a 2-D axisymmetric model to reduce computational expense. As mentioned, we also define a flow model without a consideration of the rotating screw. Note, the nozzle portion of the flow domain closely follows the geometrical design of the Model-19 extruder. However, the geometry of the screw is not available so no attempt is made to model the flow of polymer composite through the screw itself. Note that a one-inch free extrudate is longer than the typical distance between the deposition nozzle and the base plate in typical LSAM process, and thus we expect that a steady-state fiber orientation should be reached at the end of the free extrudate.

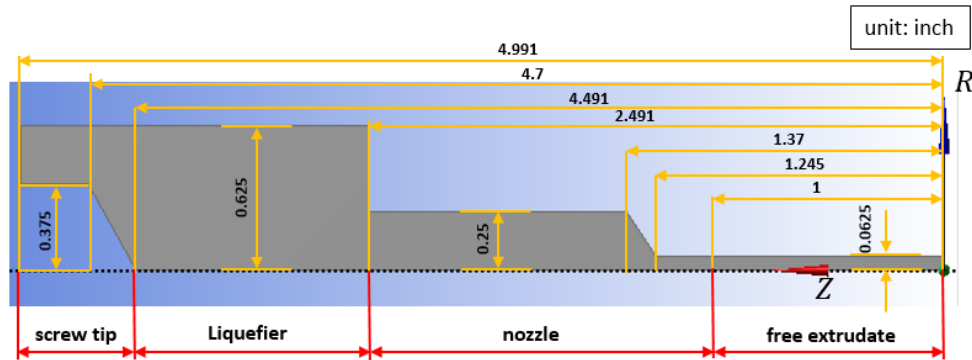


Figure 4. The dimensional information of the screw nozzle flow.

Further, an isothermal uncoupled flow assumption is applied in this study, which indicates that we neglect the fiber alignment effect as well as any non-isothermal effects when solving for the flow kinematics. These effects are beyond the main scope of our current objective, which aims to look at how screw motion affects the fiber orientation and resulting elastic properties of the bead.

Boundary conditions for the flow domain are defined as follows (see Figure 5 for the detail of flow boundaries).

- $\Gamma_1$ : Flow inlet, where the prescribed volumetric flow rate  $Q$  is specified. Also, a fully developed velocity profile is computed and imposed at the inlet by ANSYS-Polyflow based on  $Q$  and the selected rheology model. Specifically,  $Q = 400 \text{ mm}^3/\text{s}$ , resulting from a 1000 RPM input of Strangepresse Model 19 extruder.
- $\Gamma_2$ : No slip wall boundary, where  $v_s = v_n = 0$ .
- $\Gamma_3$ : Screw barrel edge, where  $v_s = v_n = 0, v_\theta = 4.2r$ . Note,  $r$  is the coordinate at  $R$  axis, as defined in Figure 3.
- $\Gamma_4$ : Axis of symmetry, where  $F_s = v_n = 0$ .
- $\Gamma_5$ : Free surface, where  $\mathbf{v} \cdot \mathbf{n} = 0$ .
- $\Gamma_6$ : Flow domain exit, where  $F_n = v_s = 0$ .

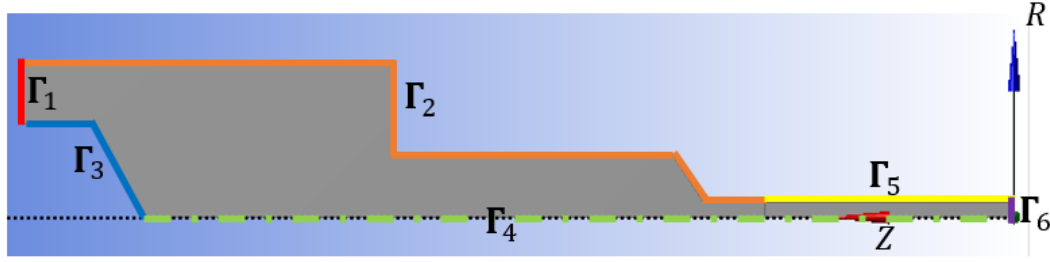


Figure 5. Boundary conditions labels of the swirling flow domain.

In the above,  $F_s$  is the tangential force,  $F_n$  is the normal force,  $v_s$  is the tangential velocity,  $v_n$  is the normal velocity,  $\mathbf{v}$  is the velocity vector at the free surface, and  $\mathbf{n}$  is a unit vector normal to the free surface. The die swell of the free surface is predicted using the methods of spines in ANSYS Polyflow [14], which is an efficient remeshing rule often applied to 2D free surface problems.

### Fiber Orientation Modeling

The orientation of a single rigid short fiber suspended in a fluid is commonly represented with the unit vector  $\mathbf{p}$  that aligns with the axis of the fiber. It is computationally prohibitive simulate the alignment of every single fiber in a fiber suspension for fiber volume fractions typical of LSAM processes. Advani, et al. [10] proposed the fiber orientation tensor to express the statistical orientation behavior of a bundle of fibers which is widely used in fiber orientation studies for polymer processing. Wang, et al. [9] extended the Advani-Tucker equation to accommodate slower orientation kinetics, which are observed in experimental works. The revised equation is written as

$$\frac{DA}{Dt} = (\mathbf{A} \cdot \mathbf{W} - \mathbf{W} \cdot \mathbf{A}) + \beta(\mathbf{D} \cdot \mathbf{A} + \mathbf{A} \cdot \mathbf{D} - 2[\mathbf{A} + (1 - \kappa)(\mathbb{L} - \mathbb{M}:\mathbf{A})]:\mathbf{D}) + \kappa C_I \dot{\gamma} (2\mathbf{I} - 6\mathbf{A}), \quad (1)$$

where

$$\mathbf{A} = A_{ij} = \oint_{\mathbb{S}} p_i p_j \Psi(\varphi, \phi) d\mathbb{S}, \quad \mathbb{A} = A_{ijkl} = \oint_{\mathbb{S}} p_i p_j p_k p_l \Psi(\varphi, \phi) d\mathbb{S} \quad (2)$$

and

$$\mathbf{W} = \frac{1}{2}[(\nabla \mathbf{v}) - (\nabla \mathbf{v})^T], \quad \mathbf{D} = \frac{1}{2}[(\nabla \mathbf{v}) + (\nabla \mathbf{v})^T] \quad (3)$$

$$\mathbb{L} = L_{ijkl} = \sum_{m=1}^3 \lambda_m \mathbf{n}_i^m \mathbf{n}_j^m \mathbf{n}_k^m \mathbf{n}_l^m, \quad \mathbb{M} = M_{ijkl} = \sum_{m=1}^3 \mathbf{n}_i^m \mathbf{n}_j^m \mathbf{n}_k^m \mathbf{n}_l^m \quad (4)$$

In the above,  $\mathbf{A}$  and  $\mathbb{A}$  are respectively the second and fourth order fiber orientation tensors, and  $\Psi(\varphi, \phi)$  is the probability distribution function which is defined over the unit sphere surface  $\mathbb{S}$ . The integral of  $\Psi(\varphi, \phi)$  over the surface  $\mathbb{S}$  equates to unity, often considered the normalization condition, which results in the trace of  $\mathbf{A}$  equating to 1 (see e.g., [10,11]). It can be shown that  $\mathbf{A}$  is symmetric which results in the second order orientation tensor consisting of five independent components which can be written as  $\mathbf{A} = A_{ij} = [A_{11}, A_{12}, A_{13}, A_{22}, A_{23}]$ . This compact form provides an efficient approach to computing fiber orientation in polymer melt flows, and will be used in our simulations below. The fourth order fiber orientation tensor  $\mathbb{A}$  is often approximated by functions of the second order orientation tensor  $\mathbf{A}$ . Previous studies have provided multiple

suggestions on the choice of a closure approximation, which include the Hybrid closure [16], the natural closure [17], the invariant-based optical-fitted closure [18], and the orthotropic closure [19]. In particular, our study will employ the orthotropic closure due to its proven numerical stability in prior similar studies [20-22].

In addition,  $\mathbf{W}$  and  $\mathbf{D}$  are the vorticity tensor and the strain rate tensor, and  $\dot{\gamma}$  is the scalar magnitude of  $\mathbf{D}$ . The velocity vector  $\mathbf{v}$  is computed along flow streamlines obtained from our ANSYS-Polyflow simulation results, and  $\nabla$  refers to the gradient operator. In addition,  $\lambda_m$  refers to the m-th eigenvalue of the second order orientation tensor and  $\mathbf{n}_i^m$  indicates the i-th component of the m-th eigenvector associated with second order orientation tensor.

The Reduced Strain Closure (RSC) model of Wang, et al. [9] incorporates the classic Isotropic Rotary Diffusion (IRD) model from Folgar, et al. [23] with an added strain reduction scale factor  $\kappa$  which acts as a closure approximation that reduces the strain effects on the orientation kinetics. For  $\kappa = 1$ , the RSC model reduces to the IRD model. Hence, we name the implemented model as the IRD-RSC model in this study since we are able to switch the two models using a different value of  $\kappa$ . Canton-Rose, et al. [24] predicted the fiber orientation of a short fiber composite injection-molded flat plate using the RSC model and found  $\kappa = 1/10$  gave the best result. Canton-Rose and Hine [25] also employed the RSC model to predict fiber orientation in short fiber composite injection molding and showed that  $\kappa=1/20$  provided the best result for slow injection rate and a fast injection rate, respectively. In addition, the effect of fiber interaction coefficient  $C_I$  was considered by Russell, et al. [26] who found that  $C_I$  ranging from 0.01 to 0.003 yielded reasonable results comparing to experimental measures in LSAM simulations. In addition, parameter  $\beta$  is a geometrical factor that is dependent on the fiber aspect ratio, and here we set it as one [9,10]. In addition, Koch, et al. [27] used a six order orientation tensor to include the influence of long-range hydrodynamic fiber interaction in semi-dilute fiber suspensions, resulting an Anisotropic Rotary Diffusion (ARD) term. Phelps, et al. [28] integrated the ARD model into the RSC model, which is suitable for predicting long fiber alignment in injection molding applications. As chopped fiber filled composites usually used in polymer additive manufacturing most likely consist of small aspect ratio short fibers, we apply the IRD-RSC model through this study.

### **Orientation Homogenized Elastic Properties Estimation**

Past developments in micromechanics models offer several analytical equations for evaluating the stiffness of unidirectionally aligned fiber reinforced polymers [12,29-31]. These unidirectional models have been applied using orientation homogenization methods (see e.g., Advani, et al. [10]) to obtain orientation averaged constitutive properties. The local orientation average stiffness  $\tilde{C}_{ijkl}$  may be written as [10]

$$\tilde{C}_{ijkl} = M_1 A_{ijkl} + M_2 (A_{ij} \delta_{kl} + A_{kl} \delta_{ij}) + M_3 (A_{ik} \delta_{jl} + A_{il} \delta_{jk} + A_{jl} \delta_{ik} + A_{jk} \delta_{il}) + M_4 A_{ij} \delta_{kl} + M_5 (A_{ik} \delta_{jl} + A_{il} \delta_{jk}), \quad (5)$$

where  $\delta_{ij}$  is the Kronecker delta [32] and the orientation tensor  $A_{ij}$  is the steady-state orientation solution, and the  $A_{ijkl}$  is computed with the orthotropic closure [19]. In addition, the values of  $M_i$  are computed as [10]

$$M_1 = C_{11} + C_{22} - 2C_{12} - 4C_{66}, M_2 = C_{12} + C_{22}, M_3 = C_{66} + 1/(2C_{22} + 2C_{23}) \\ M_4 = C_{23}, M_5 = 1/(2C_{22} - 2C_{23}) \quad (6)$$

where the  $C_{ij}$  appearing in Equations (6) are components of the stiffness tensor of the associated unidirectional fiber filled composite written in contracted notations, which we compute using the Tandon-Wang micromechanical theory [12]. It is shown by Tucker and Liang, as well as other researchers [33], that the Tandon-Wang equation [12] yields one of the most accurate estimation in elastic properties over the range of fiber aspect ratios found in the short fiber composites we are examining at present [26].

In our work, values of orientation tensor components  $A_{ij}$  are calculated along flow streamlines. Thus, the calculated  $\bar{C}_{ijkl}$  obtained at the end of each streamline is designated as the steady-state orientation state. In detail, extrudate cross-section averaged values of the effective stiffness tensor ( $\bar{C}_{ijkl}$ ) are obtained through numerical integration using the trapezoidal rule [32] as,

$$\bar{C}_{ijkl} = \frac{1}{\pi r_o^2} \int_0^{2\pi} \int_0^{r_o} \tilde{C}_{ijkl} \cdot r \, dr \, d\theta, \quad (8)$$

where  $r$  and  $\theta$  refer to the coordinates in a 2D polar system,  $r_o$  is the radius of the free extrudate end. The computed  $\bar{C}_{ijkl}$  is the computed stiffness tensor for the extruded composite. Evaluating elastic constants from the stiffness tensor  $\tilde{C}_{ijkl}$  is performed in the usual manner which is omitted here for conciseness.

## **Results and Discussions**

The effect of the screw motion on fiber orientation is discussed in this section. The flow streamlines and associated flow fields computed with our swirling flow and straight flow models are compared. A parametric study is performed to see how parameters in the fiber orientation model affect predicted fiber orientation states. In addition, the orientation-related stiffness of the composite extrudate is computed using one case of the parametric study results. Finally, a short discussion is given to integrate the presented results.

### **Flow streamline**

Streamlines within the polymer melt flow are plotted for the straight flow and the swirling flow simulations in Figure 6. Figures 6 (a) and (b) provide a planar view of the streamlines as computed by the finite element solver, ANSYS-Polyflow. Streamlines in Figure 6 (c) are obtained from the in-plane projection of the swirling flow streamlines in Figure 6 (b) with the additional angular location computed using the angular velocity provided by the finite element results. From the comparison, it is clearly seen that the screw motion yields longer streamlines than those obtained from the 2D flow kinematics alone. It can be seen that particles following the swirling streamlines traverse a significantly different path than those traveling a straight path which is expected to have a significant effect on fiber orientation in the extrudate. Additionally, a strong vorticity effect can be seen around the screw edge region and as the flow follows the screw, and the swirling becomes weaker as particles move away from the screw.

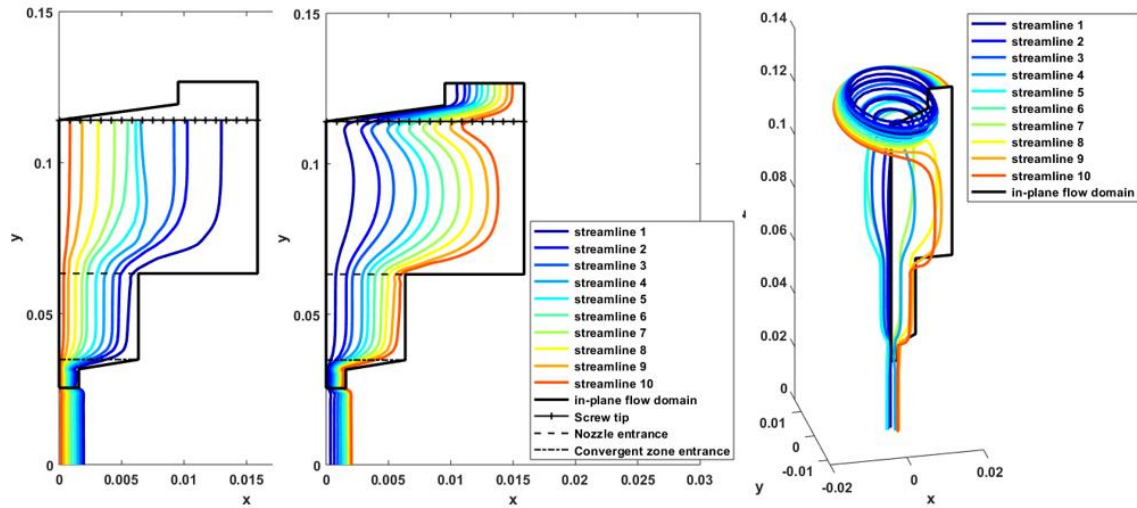


Figure 6. Flow streamlines results: (a) 2D surface streamlines from straight flow model; (b) 2D in-plane projection of streamlines from swirling flow model; (c) 3D streamlines from swirling flow model.

### ***Flow field $\dot{\theta}$ within the polymer melt flow***

The fiber orientation tensors are solved based on the flow fields along streamlines through a time integration scheme using finite difference method. A significant difference in the flow fields when comparing the straight flow and swirling flow is the kinematics associated with the angular coordinate and angular velocity. Figure 7 illustrates the flow kinematic field  $\dot{\theta}$  resulted from the swirling flow model.

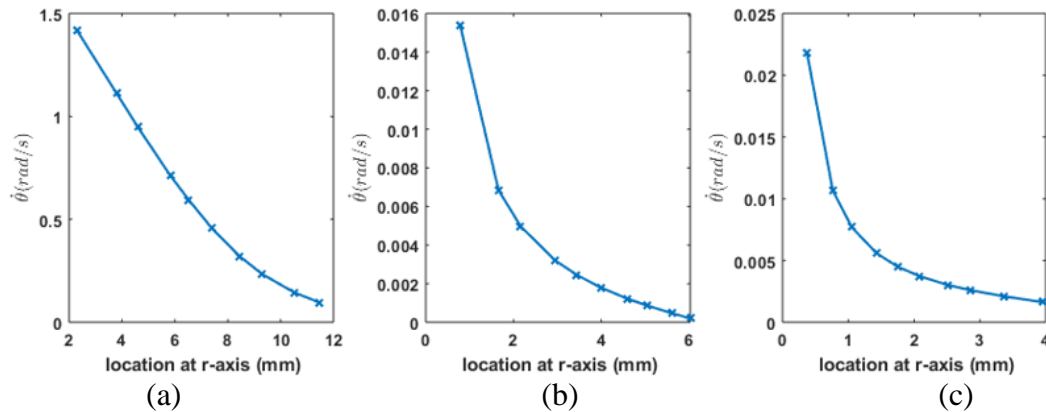


Figure 7. Flow field  $\dot{\theta}$ : (a) at the screw tip (b) at the nozzle entrance (c) at the entrance of the nozzle convergence zone (see Figure 4 for detail location information).

From Figure 7, it is seen that the swirling effects along the horizontal line at screw tip is quite strong. As the flow propagates to the nozzle entrance, the angular velocity field decays two orders of magnitude, and as the flow approaches to the convergence zone of the nozzle,  $\dot{\theta}$  reduces further as axial flow dominates the polymer motion. Thus, the influence of the swirling motion on fiber orientation kinetics most likely occurs during the region where the flow leaves the screw and before it is squeezed into the nozzle.

### **Parametric study on the fiber orientation model**

As mentioned, 1/10 and 1/20 of  $\kappa$  yield reasonable predicted fiber orientation results in injection molding applications [9,24,25,34] and thus are applied in our parametric study as well. To obtain a better understanding of the influence of  $\kappa$  on LSAM fiber orientation, we also choose  $\kappa=1$  referring the original IRD model, and  $\kappa=1/5$  as another parametric study case, besides the reported  $\kappa$  values of 1/10 and 1/20. Moreover, Russell, et al. [26] employed the IRD-RSC model when computing the Coefficient of Thermal Expansion (CTE) based on the fiber orientation prediction with fiber interaction coefficients of 0.01 and 0.003. This earlier work concluded that the predicted results are less sensitive to the change of the interaction coefficient than the choice of the scale factor  $\kappa$ . Here, we start by using the same values as Russell applied for a preliminary study. We also assume a constant geometric fiber aspect ratio,  $a_r=20$ , which is a common value seen in the material model we selected (13% CF-ABS). In addition, it is important to note that the initial condition for  $A_{ij}$  is vital for a fiber orientation evaluation. We assume an isotropic fiber alignment at the inlet of our flow domains.

The predicted fiber orientation states appearing in Figure 8 are the orientation tensor values at the end of the flow streamlines, where we consider a steady-state flow-induced fiber orientation occurs. For conciseness, the orientation tensor component that indicates the fiber alignment parallel to the extrusion direction (z-axis) are given. In the case of  $C_I=0.01$ , the standard IRD model ( $\kappa=1$ ) does not indicate much difference between the two flow models. However, a significant deviation is seen between the two flow model predictions as the RSC model is applied with three different non-unity values of  $\kappa$ . In detail, the swirling flow model yields high fiber alignment along the extrusion direction while the principal orientation status predicted by the straight flow decreases with decreasing values of  $\kappa$ . It can be seen that values of  $A_{ij}$  for  $C_I=0.003$  show a similar trend as those obtained in the case of  $C_I=0.01$ , except that a sudden spike occurs in the predicted result near the shear dominant boundary, especially for the results from the swirling flow.

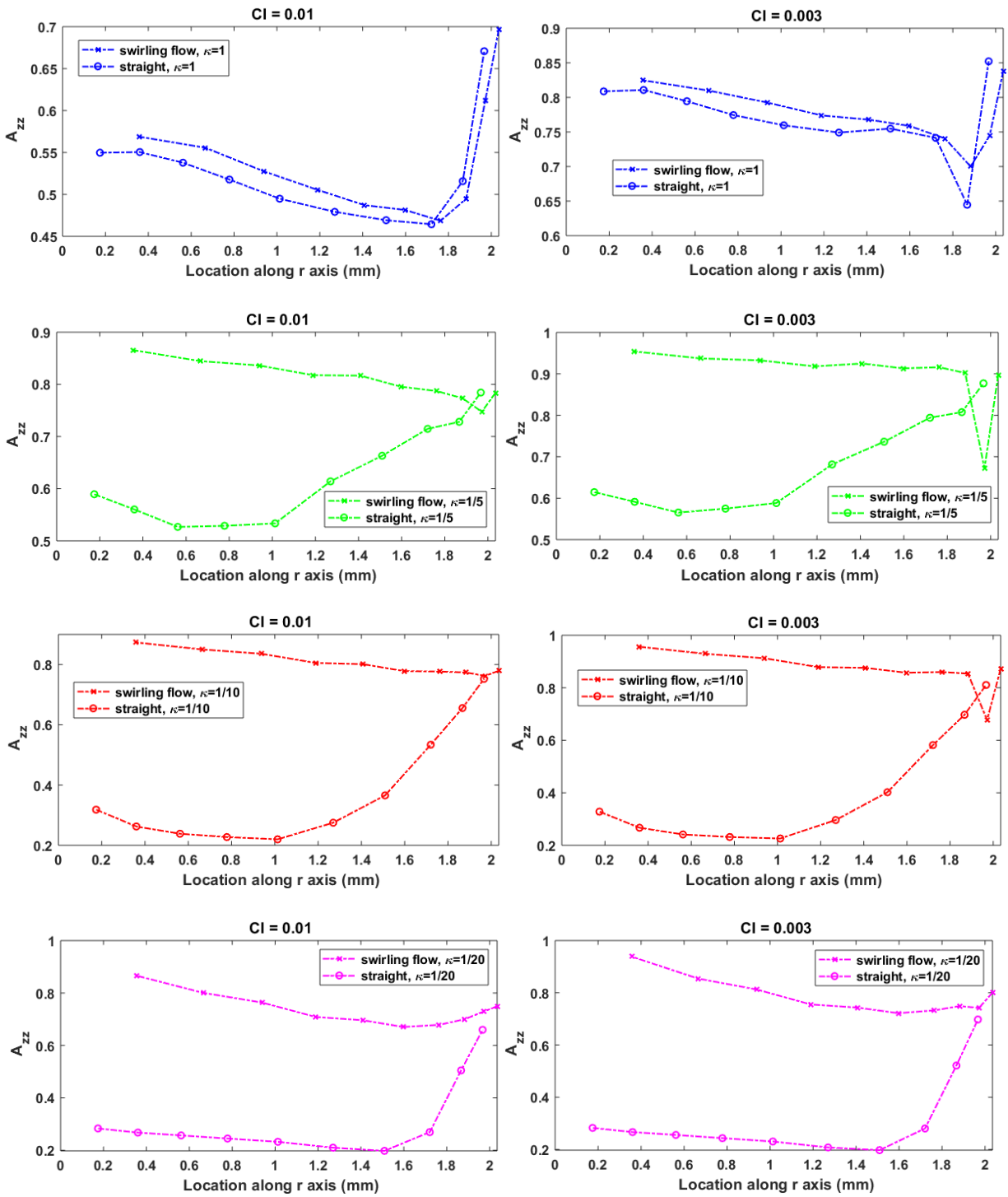


Figure 8. Steady-state fiber orientation parallel to the extrusion direction ( $A_{zz}$  component): parametric study on  $\kappa$  and  $C_I$ .

### Homogenized effective stiffness

To further explore effects of the orientation model parameters, we use the steady-state orientation tensors (i.e., those obtained at the flow domain exit) to evaluate the cross-section averaged elastic constants with the orientation homogenization method [10-12] described above. The composite material system we consider contains 13% by volume carbon fiber reinforced ABS composite where elastic constants of the fiber and matrix phases are given through Table 3. Notice, we assume both the carbon fiber and the ABS are isotropic materials. Russell, et al. [26] indicated that the orientation-related effective elastic properties are more sensitive to the selection of the strain scale factor than that of the fiber interaction coefficient when computing the CTE of the deposited bead. A similar trend can be seen in Figure 7, where steady-state orientation states shows more variation with applied scale factor  $\kappa$  than that of the interaction coefficient. In particular, the elastic constants estimated through the data resulted from the case of  $C_I=0.01$  are given in Table 4. In addition, the geometric fiber aspect ratio used in obtaining following results is 20. Generally, the values appearing in Table 4 are supported by results shown in Figure 8. In most of the cases considered here, the stiffness parallel to the principal extrusion direction is higher than those at transverse directions. Particularly, the swirling-flow-predicted elastic behaviors remain anisotropy and the stiffness along the principle direction is much higher than those at transverse directions even a small  $\kappa$  is imposed, while the results from the straight flow convert from highly anisotropy to quasi-isotropic at  $\kappa=1/10$  and the moduli at transverse directions become even higher than that at the principle direction at  $\kappa=1/20$ .

Table 3. Elastic properties for a 13% carbon fiber reinforced ABS composite [22].

Material	$E$ (GPa)	$\nu$
Carbon fiber	230	0.2
ABS matrix	2.1	0.35

Table 4. Homogenized elastic moduli predicted by the swirling and straight flow models. Note,  $C_I=0.01$  in this case. The extrusion direction is parallel to the  $z$  axis, which is considered as the principal direction,  $r$  and  $\theta$  are referred the transverse directions.

Flow model	$\kappa$	$E_{rr}$ (GPa)	$E_{zz}$ (GPa)	$E_{\theta\theta}$ (GPa)
Swirling flow	1	3.75	6.67	4.33
Swirling flow	1/5	3.02	10.30	3.26
Swirling flow	1/10	2.94	10.06	3.41
Swirling flow	1/20	2.96	8.39	3.83
Straight flow	1	3.72	6.32	4.27
Straight flow	1/5	3.30	6.88	3.57
Straight flow	1/10	4.40	4.44	3.95
Straight flow	1/20	5.30	4.06	4.27

### Discussion

Significant difference between flow fields of the swirling flow and the straight flow yields angular velocity, where the kinematics of the swirling flow is shown in Figure 7 and that of the straight flow are all zero. From the computed results shown above, it can be seen that the interaction of the swirling motion and the fiber orientation within the flow region near the screw

tip is most likely not captured by the standard IRD model, as the IRD-predicted fiber orientation kinetics evolve quickly, reaching a quasi-steady state before the flow approaching the nozzle entrance [26]. Hence, subtle differences are seen in the predicted steady-state orientation tensor and the associated stiffness when  $\kappa=1$  is applied (corresponding to standard IRD-model). As the RSC-model is incorporated by decreasing the  $\kappa$  value, a distinct deviation between the results from the two flow models becomes apparent. This indicates that the swirling effect has been taken into account as the fiber orientation evolves through the flow. Specifically, a smaller  $\kappa$  yields a slower rate of orientation evolution. Duty, et al. [7] reported that a high degree of anisotropy was found in the measured stiffness of the fiber reinforced composites printed through LSAM applications. We can see that the elastic properties predicted by the swirling flow exhibit an anisotropic behavior regardless of the applied values of  $\kappa$  and  $C_I$ , while those predicted by the straight flow convert from high anisotropy to quasi-isotropy as  $\kappa$  decreases, which contradicts to the experimental observation. In additional, Duty also provided the stiffness of a 13% CF-ABS bead printed by a LSAM system, in which the tensile modulus along the printing direction was found at 8.18 GPa with a standard deviation of 0.37. Our computed results using the swirling flow model yields in a similar predicted value of 8.39 GPa at  $\kappa=1/20$  and  $C_I=0.01$  for the elastic modulus along the extrusion direction. While the simulation presented in this paper does not specifically represent the experimental setup in Duty's work [7], the preliminary comparison still implies that the flow model considering the swirling motion effects yields a more reasonable estimation for elastic properties of a printed fiber reinforced polymer material.

### **Conclusion**

This paper investigates the screw swirling effects on predicted fiber orientation and associated effective elastic properties of a composite extrudate in LSAM polymer deposition. A weakly coupled one-way analysis is performed in flow and fiber orientation computation. The finite element method is used to simulate the polymer melt flow within the screw tip and nozzle region. The IRD-RSC model is applied to solve the fiber orientation state with computed kinematics of the uncoupled flows. It is found that the standard IRD model does not capture the effect of rotational kinematics on fiber orientation while the IRD-RSC model is able to characterize the screw motion impact on the resulting fiber orientation with difference values of modeling parameters. Specifically, the strain reduction scale factor is of significant importance in determining the resulting predicted orientation states.

The swirling flow model is also able to reflect the material anisotropy of an extruded composite regardless of the choice of the scale factor while the straight flow model yields a quasi-isotropic elastic constants prediction when a small value of scale factor is assigned, which is contradictory to prior experimental measurements. Also, the swirling flow provides a reasonable prediction with certain orientation modeling parameters for the principle stiffness of an extruded fiber filled polymer, which shows good agreement with prior experimental study.

### **Future Work**

A corresponding experimental measurement for the orientation state of an extruded composite bead is in need, by which we can fit the essential parameters for the applied orientation evaluation model with more accuracy. Another valuable verification of our study is to measure the tensile moduli of printed composite extrudates and compare with the predicted effective stiffness.

## Acknowledgements

The authors would like to thank Baylor University for the financial support on this project. Also, we want to thank the Strangpresse Corporation for donating their Model-19 extruder for our research usage.

## References

- [1] Zhou, et al. "Numerical simulation for exploring the effect of viscosity on single-screw extrusion process of propellant." *Procedia Engineering* 84 (2014): 933-939.
- [2] Michelangelli, O. P., et al. "Modelling pellet flow in single extrusion with DEM." *Proceedings of the Institution of Mechanical Engineers, Part E: Journal of Process Mechanical Engineering* 225.4 (2011): 255-268.
- [3] Canevarolo, Sebastião V., and Ana Clélia Babetto. "Effect of screw element type in degradation of polypropylene upon multiple extrusions." *Advances in Polymer Technology: Journal of the Polymer Processing Institute* 21.4 (2002): 243-249.
- [4] Kelly, Adrian L., Elaine C. Brown, and Philip D. Coates. "The effect of screw geometry on melt temperature profile in single screw extrusion." *Polymer Engineering & Science* 46.12 (2006): 1706-1714.
- [5] Ramani, Karthik, Dave Bank, and Nick Kraemer. "Effect of screw design on fiber damage in extrusion compounding and composite properties." *Polymer composites* 16.3 (1995): 258-266.
- [6] Covas, José A., et al. "Evolution of Chemistry, Morphology and Rheology of Various Polymer Systems along a Twin-Screw Extruder." *The Canadian Journal of Chemical Engineering* 80.6 (2002): 1065-1074.
- [7] Duty, Chad E., et al. "Structure and mechanical behavior of Big Area Additive Manufacturing (BAAM) materials." *Rapid Prototyping Journal* 23.1 (2017): 181-189.
- [8] Tucker CL. Flow regimes for fiber suspensions in narrow gaps. *Journal of Non-Newtonian fluid mechanics*. 1991 Jan 1;39(3):239-68.
- [9] Wang, Jin, John F. O'Gara, and Charles L. Tucker III. "An objective model for slow orientation kinetics in concentrated fiber suspensions: Theory and rheological evidence." *Journal of Rheology* 52.5 (2008): 1179-1200.
- [10] Advani SG, Tucker III CL. The use of tensors to describe and predict fiber orientation in short fiber composites. *Journal of rheology*. 1987 Nov;31(8):751-84.
- [11] Jack, David Abram. *Advanced analysis of short-fiber polymer composite material behavior*. Diss. University of Missouri--Columbia, 2006.
- [12] Tandon GP, Weng GJ. The effect of aspect ratio of inclusions on the elastic properties of unidirectionally aligned composites. *Polym Compos* 1984;5:327-33.
- [13] Thien, Nhan Phan, and Roger I. Tanner. "A new constitutive equation derived from network theory." *Journal of Non-Newtonian Fluid Mechanics* 2.4 (1977): 353-365.
- [14] ANSYS POLYFLOW User's Guide, Ansys Inc., 2013.
- [15] Cox, W. P., and E. H. Merz. "Correlation of dynamic and steady flow viscosities." *Journal of Polymer Science* 28.118 (1958): 619-622.
- [16] Advani, Suresh G., and Charles L. Tucker III. "Closure approximations for three-dimensional structure tensors." *Journal of Rheology* 34.3 (1990): 367-386.
- [17] De Frahan, H. Henry, et al. "Numerical prediction of fiber orientation in injection molding." *Polymer Engineering & Science* 32.4 (1992): 254-266.
- [18] Chung, Du Hwan, and Tai Hun Kwon. "Fiber orientation in the processing of polymer composites." *Korea-Australia Rheology Journal* 14.4 (2002): 175-188.
- [19] Cintra Jr, Joaquim S., and Charles L. Tucker III. "Orthotropic closure approximations for flow-induced fiber orientation." *Journal of Rheology* 39.6 (1995): 1095-1122.

- [20] VerWeyst, Brent E., and Charles L. Tucker III. "Fiber suspensions in complex geometries: flow/orientation coupling." *The Canadian Journal of Chemical Engineering* 80.6 (2002): 1093-1106.
- [21] Heller, Blake P., Douglas E. Smith, and David A. Jack. "Effects of extrudate swell and nozzle geometry on fiber orientation in Fused Filament Fabrication nozzle flow." *Additive Manufacturing* 12 (2016): 252-264.
- [22] Wang Z, Smith D E. Rheology Effects on Predicted Fiber Orientation and Elastic Properties in Large Scale Polymer Composite Additive Manufacturing [J]. *Journal of Composites Science*, 2018, 2(1): 10.
- [23] Folgar, Fransisco, and Charles L. Tucker III. "Orientation behavior of fibers in concentrated suspensions." *Journal of reinforced plastics and composites* 3.2 (1984): 98-119.
- [24] Caton-Rose, P., et al. "MEASUREMENT AND PREDICTION OF SHORT GLASS FIBRE ORIENTATION IN INJECTION MOULDING COMPOSITES." *European Conference on Composite Materials*. Vol. 15. 2012.
- [25] Caton-Rose, F., P. Hine, and B. Parveen. "Prediction of fibre orientation in short glass fibre reinforced composite injection moulding." *International Conference of Composite Materials* 16, Montreal, Canada.
- [26] Russell, Timothy, et al. "Prediction of the Fiber Orientation State and the Resulting Structural and Thermal Properties of Fiber Reinforced Additive Manufactured Composites Fabricated Using the Big Area Additive Manufacturing Process." *Journal of Composites Science* 2.2 (2018): 26.
- [27] Koch, Donald L. "A model for orientational diffusion in fiber suspensions." *Physics of Fluids* 7.8 (1995): 2086-2088.
- [28] Phelps, Jay H., and Charles L. Tucker III. "An anisotropic rotary diffusion model for fiber orientation in short-and long-fiber thermoplastics." *Journal of Non-Newtonian Fluid Mechanics* 156.3 (2009): 165-176.
- [29] Mori T, Tanaka K. Average stress in matrix and average elastic energy of materials with misfitting inclusions. *Acta Metallurgica* 1973;21:571-4.
- [30] Halpin JC. Stiffness and Expansion Estimates for Oriented Short Fiber Composites. *J Compos Mater* 1969;3:732-4.
- [31] Laws N, McLaughlin R. The effect of fibre length on the overall moduli of composite materials. *J Mech Phys Solids* 1979;27:1-13
- [32] Chapra, Steven C. "Applied numerical methods." *With MATLAB for Engineers and Scientists* (2012).
- [33] Tucker III, Charles L., and Erwin Liang. "Stiffness predictions for unidirectional short-fiber composites: review and evaluation." *Composites science and technology* 59.5 (1999): 655-671.
- [34] Wang, Jin, and Xiaoshi Jin. "Comparison of recent fiber orientation models in autodesk moldflow insight simulations with measured fiber orientation data." *Polymer Processing Society 26th Annual Meeting*. Canada: Banff, 2010.